Unified Online Estimation Method for SOC, SOH, and Power Capacity Considering Safety Boundary Consistency in Battery Management Systems

Dan Xu *, Huangyin Chen , Hao Gui

Posted Date: 2 March 2026

doi: 10.20944/preprints202603.0079.v1

Keywords: battery management system; state of charge; state of health; power capacity; unified estimation; safety boundary; dual-extension Kalman filter; data-driven modeling; parameter evolution; wide temperature range operating conditions

 doi:10.20944/preprints202603.0079.v1

Article

Unified Online Estimation Method for SOC, SOH, and Power Capacity Considering Safety Boundary Consistency in Battery Management Systems

Dan Xu [1,*], Huangyin Chen [2] and Hao Gui [3]

[1] Rivian, Tustin, United States
[2] Johns Hopkins University, Baltimore, MD, USA
[3] GE HealthCare
* Correspondence: danxu2017@gmail.com

Abstract

Under high C-rate and wide-temperature conditions, independently estimated SOC and SOH often diverge due to decoupled model dynamics, resulting in inaccurate power boundary calculations. This affects power limiting, thermal safety, and fast-charging strategies. To solve this, a unified online estimation framework is proposed for SOC, SOH, and power capacity under voltage and thermal constraints. It integrates a state-space model based on an equivalent circuit, combining SOC, polarization voltage, internal resistance, and capacity degradation, with temperature-dependent parameter evolution to capture coupling with aging. A dual extended Kalman filter enables collaborative SOC–SOH estimation, while lightweight machine learning modules correct internal resistance and polarization dynamics to reduce mismatch under extreme conditions. Physical constraint projections embed voltage, temperature, and power limits into the estimation loop, mitigating noise amplification and drift. Based on consistent estimates, the SOP boundary is computed online to support control decisions. Validation across six temperatures (−20 °C to 55 °C) and five C-rates (0.2C to 6C), using bench, HIL, and pack-level tests over 120+ hours, shows SOC RMSE <1.6%, SOH error <2.5%, and SOP hit rate >95% within 10 seconds. Under noise and parameter disturbances, error growth is reduced by ~25% versus baselines. These results confirm improved SOC–SOH consistency and boundary tracking, with computational cost suitable for embedded deployment.

Keywords: battery management system; state of charge; state of health; power capacity; unified estimation; safety boundary; dual-extension Kalman filter; data-driven modeling; parameter evolution; wide temperature range operating conditions

1. Introduction

With the rapid deployment of energy storage systems and more frequent extreme weather, battery management systems (BMS) face increasing demands to shift from steady-state monitoring to dynamic safety regulation. The estimation accuracy and consistency of core state variables—state of charge (SOC), state of health (SOH), and power capability—are critical to vehicle safety and reliability. Under high C-rate and wide-temperature conditions, these states show strong coupling, nonlinearity, and time variance, making traditional independent estimation methods insufficient. They often fail to capture inter-state dynamics, leading to inaccurate power boundary predictions and compromised thermal and energy management. Existing studies largely improve single-state estimation but lack unified models and feedback mechanisms to ensure consistency across states. To address this, a unified estimation framework is needed—one that jointly models SOC, SOH, and power capability while embedding safety boundaries—to support stable and interpretable control under complex operating scenarios.

 doi:10.20944/preprints202603.0079.v1

2. Design of Unified Online Estimation Algorithm for SOC, SOH, and Power Capacity

2.1. Construction of a Unified State Space Model

To enable unified perception and closed-loop control of battery state of charge (SOC), state of health (SOH), and available power capability under high C-rate and wide-temperature operating conditions, a state-space model that preserves physical consistency and inter-state coupling is required [1]. The construction of a unified state-space model is specifically aimed at capturing the intrinsic coupling relationships among multiple battery states, including SOC, SOH, polarization voltage, and internal resistance. These states exhibit interdependent and time-varying dynamics, particularly under rapid charging/discharging or thermal fluctuations. For example, internal resistance variations due to aging directly affect the voltage response and hence SOC estimation accuracy, while polarization voltage dynamics are also modulated by both temperature and capacity degradation. To reflect such interactions systematically, a unified state vector is formulated based on a first-order equivalent circuit model. Accordingly, the state vector is defined as:

$$x(k) = \left[SOC(k), U_p(k), R_{\text{int}}(k), C_{fade}(k)\right]^T$$

where $U_p(k)$ denotes polarization voltage, $R_{\text{int}}(k)$ represents current internal resistance, and $C_{fade}(k)$ indicates relative capacity degradation. All variables dynamically evolve within the estimation framework. The inputs include current I(k) and temperature T(k) at the current time step, while the observed variable is the terminal voltage Uterm(k). The temperature factor influences R_{int} and C_{fade} through a parameter evolution model, thereby capturing the coupling between aging behavior and operating conditions. Meanwhile, U_p is linked to SOC via a dynamic voltage equation. During state transitions, process noise terms are introduced to account for sensor drift and abrupt operating condition changes, improving the robustness of the estimation process. Since temperature drives the evolution of internal resistance and capacity degradation, its measurement errors can propagate through parameter updates and affect SOC–SOH consistency. To address this, the model incorporates temperature-channel uncertainty into the dual-EKF process noise matrix, enabling adaptive gain adjustment based on input reliability. Additionally, the constraint projection in Section 2.4 corrects deviations from temperature-induced drifts, helping suppress noise amplification and maintain robustness under real-world thermal conditions. The overall state coupling structure, illustrated in Figure 1, enables information fusion across multiple state dimensions and provides the structural basis for collaborative estimation using a dual extended Kalman filtering framework.

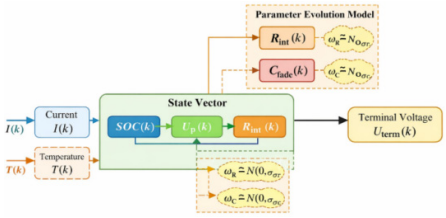

Figure 1. Schematic of Unified State Space Coupling.

2.2. Dual Extended Kalman Filter Cooperative Estimation Framework

Traditional single extended Kalman filters struggle to capture both short-term dynamics and long-term aging patterns in battery cells, often causing cross-interference and reduced estimation stability. To address this, a dual extended Kalman filtering (dual-EKF) approach is adopted to decouple and balance the estimation of fast-changing states (e.g., SOC and polarization) and slowly

 doi:10.20944/preprints202603.0079.v1

evolving aging states (e.g., internal resistance and capacity fade). Short-term dynamics respond rapidly to load and temperature changes, while aging states exhibit quasi-static behavior. Estimating both with a single filter compromises performance. The dual-EKF structure resolves this by introducing asynchronous updates and feedback coupling. A primary SOC filter tracks transient states, while an auxiliary SOH filter estimates long-term health parameters, ensuring consistent and interpretable state tracking [2]. In the SOC filter, state transitions are based on the coupled dynamics of SOC and polarization voltage, with updates driven by terminal voltage residuals. The SOH filter tracks internal resistance and capacity decay quasi-statically, using current temperature and historical data. An internal resistance feedback channel links the two filters, allowing SOH estimates to correct voltage response parameters in the SOC filter. This ensures consistent fusion of short-term dynamics and long-term degradation. Figure 2 shows the architecture of the dual-EKF structure, including state subspace boundaries, observation channel allocation, and covariance propagation paths designed to maintain stability and observability under wide temperature and high C-rate conditions [3].

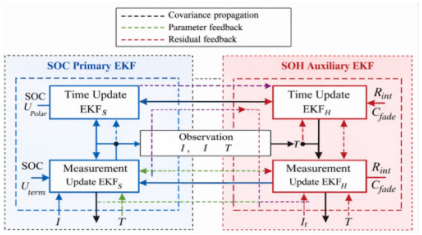

Figure 2. Schematic of Dual EKF Information Exchange and Collaborative Update.

2.3. Adaptive Correction and Residual Compensation in the Data-Driven Module

To address model mismatches under high C-rate and extreme temperature conditions, a data-driven module is embedded in the measurement update phase of the dual-EKF framework. In such scenarios, battery parameters like polarization resistance, diffusion dynamics, and ohmic losses vary rapidly and nonlinearly, making them difficult to model accurately with traditional equivalent circuits. This leads to systematic voltage prediction errors, causing estimation bias and filter instability. A compact feedforward neural network (FNN) is introduced as a residual regression module, trained online to approximate unmodeled dynamics and condition-dependent deviations between observed and predicted terminal voltages. Acting as a correction layer, the FNN selectively compensates for high-rate and thermal modeling errors while preserving the interpretability and stability of the dual-EKF structure. The voltage residual $\tilde{e}(k) = U_{term}(k) - \hat{U}_{model}(k)$ is decomposed into a learnable bias component and a random noise component:

$$\delta(k) = N_\theta(X(k)), \quad \hat{U}_{corrected}(k) = \hat{U}_{model}(k) + \delta(k)$$

where $N_\theta(k)$ denotes a lightweight neural network parameterized by weights θ, receiving as input a time-dependent feature vector $X(k) = [I(k), T(k). S\hat{O}C(k), V_p(k), \mu_e(k)]$, which integrates current, temperature, prior SOC estimate, polarization voltage state, and the sliding mean of historical residuals $\mu_e(k)$. This module operates under a recursive least-squares error minimization scheme with exponential forgetting, enabling continuous online adaptation of θ without interrupting filter operation.

To maintain filter stability and bounded gain dynamics, the corrected voltage estimate $\hat{U}_{corrected}(k)$ is used to update the observation function within the SOC filter, while a data-driven adaptive noise estimation mechanism jointly adjusts the covariance matrix R(k) based on the statistical trend of $\tilde{e}(k)$. The lightweight neural network used for residual compensation is shown in Figure 3. It adopts a compact feedforward structure with a low-dimensional input layer, a single hidden layer, and an output layer generating voltage residual corrections. Inputs include current, temperature, estimated SOC, polarization voltage, and residual statistics from the unified estimation process.

 doi:10.20944/preprints202603.0079.v1

As shown in Figure 3, the network output feeds into the SOC filter's voltage observation channel, forming a closed-loop correction without altering the original state transition. This auxiliary design compensates for nonlinear, condition-dependent errors while preserving the stability and interpretability of the dual-EKF framework.

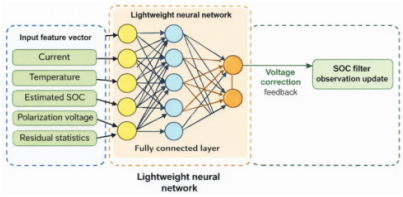

Figure 3. Lightweight neural network for voltage residual compensation and EKF integration.

2.4. Physical Constraint Projection and Consistency Control Mechanism

To prevent SOC and SOH estimates from drifting beyond the battery's feasible domain under high-rate and strong-coupling conditions, a physical constraint projection and consistency control mechanism is added during state updates. It maps voltage, temperature, and power capability constraints into the state space for closed-loop enforcement [5]. Specifically, after each filtering update, the feasible state domain $\Omega_k = \{x_k \mid V_{\min} \le g_V(x_k, I_k, T_k) \le V_{\max}, T_k \le V_{\max}\}$ is first constructed based on the equivalent circuit and power capability models, where x_k is the joint state vector containing SOC, SOH, and polarization states, and g_V represents the terminal voltage expression derived from the state mapping. Subsequently, the estimated state is projected onto this feasible domain through weighted distance minimization:

$$x_k^p = \arg\min_{x \in \Omega_k} (x - x_k)^T P_k^{-1} (x - x_k)$$

where P_k denotes the filtering covariance matrix, which maintains statistical consistency and prevents overcorrection of high-confidence states. The projection serves as an intermediate variable for consistency control, feeding back into SOC–SOH updates and power capability calculations. It ensures coherent evolution of state estimates, power boundaries, and safety constraints [6]. Figure 4 shows the trajectory converging onto the constraint space, highlighting the constraint mechanism's role within the unified framework as a stable basis for online power boundary computation.

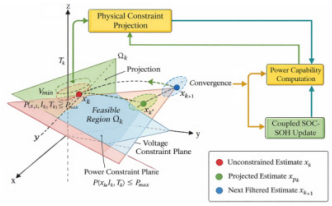

Figure 4. Projection of state estimation in the constraint space and convergence illustration.

3. Online SOP Safety Boundary Calculation and Control Interface Based on Consistent Estimation

3.1. Power Capacity Calculation Driven by Consistent SOC–SOH Results

Based on the unified SOC–SOH estimation after constraint projection, the power capability module adopts a "state consistency priority" principle. It integrates SOC, SOH, and internal resistance evolution into SOP calculation, avoiding mismatches common in traditional methods [7]. The module updates equivalent capacity (Ceq) and ohmic resistance (R0) using consistent estimates, then combines polarization and terminal voltage predictions to determine a current interval

 doi:10.20944/preprints202603.0079.v1

satisfying voltage and thermal constraints. On this basis, the discharge power capability is computed online using the following formula:

$$P_{\max,k} = I_{\max,k} \cdot \left(V_{oc}(z_k, h_k) - I_{\max,k} R_0(h_k, T_k) - V_{\min}\right)$$

where z_k and h_k denote the unified SOC and SOH estimates, respectively; V_{oc} is the open-circuit voltage mapping function; T_k represents the battery temperature state; $V_{\min}$ is the safe voltage lower bound; and $I_{\max,k}$ is obtained through constraint-consistent state prediction back-solving. This process relies on the unified state vector, ensuring the power boundary evolves consistently with SOC and SOH, and provides a clear, interpretable basis for SOP updates and control execution [8].

3.2. Application of SOP Safety Boundary in BMS Control

At the BMS control level, the SOP boundary functions as a dynamic constraint within the power command loop, driven by consistent SOC–SOH estimates. This enables real-time adaptive power control as battery states evolve [9]. The computed charge and discharge SOP limits serve as upper bounds in the control process. After the power command P_{req} is generated by the drive, motor, or charge controller, the BMS performs command shaping through a boundary consistency verification module. Its control law can be uniformly expressed as

$$P_{cmd} = sat(P_{req}, -P^{chg}_{\max,k}, P^{dis}_{\max,k})$$

where $P^{chg}_{\max,k}$ and $P^{dis}_{\max,k}$ represent the online-updated charging and discharging safe power boundaries based on consistent estimation, respectively. The operator sat enforces upper and lower bounds, keeping execution power within limits defined by voltage, temperature, and health status. This avoids the drawbacks of fixed SOC or voltage-based strategies, enabling power control to adapt to SOC degradation, internal resistance changes, and operating conditions. Through a unified interface, it delivers continuous, interpretable power commands to execution units, ensuring consistent safety references for vehicle energy and thermal management [10].

4. Experimental Design and Validation Analysis

4.1. Experimental Platform and Dataset Construction

To validate the proposed unified estimation method under wide-temperature and high C-rate conditions, a hybrid platform combining a programmable bench-test system and hardware-in-the-loop (HIL) was established. The setup includes a high-precision load, multi-channel current/voltage/temperature acquisition modules, and a thermal chamber (−30 °C to 60 °C).

Figure 5 shows the platform, integrating the battery module, thermal chamber, programmable load, DAQ unit, NI PXI HIL controller, and CAN-based BMS interface. The test battery, placed in the thermal chamber, is connected to the load and controller for synchronized data acquisition and real-time control.

Commercial 18650 ternary lithium-ion cells at various aging stages were tested under diverse stress profiles. Table 1 summarizes the setup and data attributes. The dataset covers six temperature points and five C-rate ranges, combining static and dynamic protocols, and supports filter calibration, parameter evolution, and SOP boundary evaluation across thermal–electrical conditions.

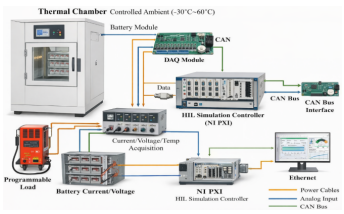

Figure 5. Schematic Diagram of Experimental Setup.

 doi:10.20944/preprints202603.0079.v1

Table 1. Experimental Configuration and Dataset Overview.

Parameter Category	Configuration Details
Cell Type	18650 Ternary Lithium-ion
Temperature Range	−20 °C, −10 °C, 0 °C, 25 °C, 40 °C, 55 °C
Charge/Discharge Rates	0.2C, 1C, 2C, 4C, 6C
Test Types	CC-CV Charging, Dynamic FUDS/UDDS, Pulse Load
Total Duration	>120 hours (bench + HIL)
Measured Features	Voltage, Current, Temperature, SOC, SOH, Cell ID, Time Stamps
HIL Configuration	Real-time NI PXI System, CAN Bus Interface, Closed-loop Execution

4.2. Results Analysis and Discussion

Validation experiments used the hybrid dataset from Section 4.1, covering six temperatures (−20 °C to 55 °C) and five discharge rates (0.2C to 6C), reflecting typical EV conditions. The goal was to evaluate the framework's accuracy, robustness, and boundary consistency under thermal-electric disturbances and dynamic loads. Figure 6 shows SOC and SOH error convergence after constraint projection. Under extreme conditions (e.g., 4C at −10 °C), initial estimates deviate significantly but gradually converge within the feasible region through dual-EKF updates with residual correction and feedback—demonstrating effective drift suppression and statistical consistency. For benchmarking, the method was compared against (i) a conventional single-EKF and (ii) a dual-EKF without machine learning. Metrics included SOC RMSE, SOH relative error, and 10-second SOP hit rate. As shown in Figure 7 and the table, the proposed method outperforms both baselines. The integrated neural model notably reduces voltage tracking errors and gain instability, improving SOC–SOH consistency. A SOP hit rate above 96% confirms accurate power boundary tracking under thermal and aging stress, validating its suitability for control-oriented BMS applications.

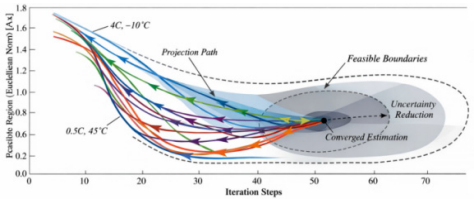

Figure 6. Projected convergence trajectory of SOC-SOH estimation.

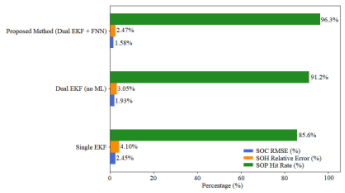

Figure 7. Comparative Estimation Accuracy Across Methods.

5. Conclusions

The proposed unified state sensing and safety boundary fusion method marks a shift from independent diagnostics to consistency-driven control under coupled, multi-disturbance conditions. By combining a physically coupled state-space model with dual extended Kalman filtering and data-driven residual compensation, the approach enables consistent estimation of SOC, SOH, and power capability, enhancing safety boundary observability and control reliability. While simulation and experimental results are promising, challenges remain in parameter generalization and failure

 doi:10.20944/preprints202603.0079.v1

response. The method's adaptability to various cell chemistries and formats requires further study. Future work will explore lightweight model design and edge deployment to support multi-scenario, multi-level BMS architectures, enabling adaptive energy and health management from cell to system level.

References

1. Chen, X., Huang, Y., Jessney, B., Sangha, J., Gu, S., Schönlieb, C. B., ... & Roberts, M. (2025). Review and recommendations for using artificial intelligence in intracoronary optical coherence tomography analysis. European Heart Journal-Digital Health, ztaf053.
2. Hu P, Tang W F, Li C H, et al. Joint state of charge (SOC) and state of health (SOH) estimation for lithium-ion battery packs of electric vehicles based on NSSR-LSTM neural network[J]. Energies, 2023, 16(14): 5313.
3. Zeng X, Sun Y, Xia X, et al. A framework for joint SOC and SOH estimation of lithium-ion battery: eliminating the dependency on initial states[J]. Applied Energy, 2025, 377: 124624.
4. Ye Z, Deng Z H, Xu Y H, et al. Joint estimation of SOC and SOH for lithium-ion batteries based on FOAMIUHF-UKF model[J]. Scientific Reports, 2025, 15(1): 40743.
5. Wei Z, Sun X, Li Y, et al. A Joint Estimation Method for the SOC and SOH of Lithium-Ion Batteries Based on AR-ECM and Data-Driven Model Fusion[J]. Electronics, 2025, 14(7): 1290.
6. Dong Y, Zhang G, Li R. Comparative Study of Joint Estimation of State of Charge (SOC) and State of Health (SOH) of Lithium-ion Batteries Based on Different Tree Models[J]. Journal of Electrical and Electronic Engineering, 2024, 12(2): 23-35.
7. Tao J, Wang S, Cao W, et al. A comprehensive review of state-of-charge and state-of-health estimation for lithium-ion battery energy storage systems[J]. Ionics, 2024, 30(10): 5903-5927.
8. Zhou R, Zhu R, Huang C G, et al. State of health estimation for fast-charging lithium-ion battery based on incremental capacity analysis[J]. Journal of Energy Storage, 2022, 51: 104560.
9. Roy P K, Shahjalal M, Shams T, et al. A critical review on battery aging and state estimation technologies of lithium-ion batteries: prospects and issues[J]. Electronics, 2023, 12(19): 4105.
10. Bustos R, Gadsden S A, Al-Shabi M, et al. Lithium-ion battery health estimation using an adaptive dual interacting model algorithm for electric vehicles[J]. Applied Sciences, 2023, 13(2): 1132.